An Improved Approach for Structural Delineation with Multiple Reverse Faults from Borehole Image Dips in Compressional Stress Regime*

Shiduo Yang[1], Yang Yang[2], Yafeng Li[2], Guo Wei[1], Alexis He[1], Isabelle Le Nir[1], Tetsushi Yamada[1], Fangfang Wu[1], Mo jing[1], and Mohamed Ahmed Alboub[1]

Search and Discovery Article #42335 (2018)**
Posted December 31, 2018

*Adapted from extended abstract based on poster presentation given at 2018 International Conference and Exhibition, Cape Town, South Africa, November 4-7, 2018. Please see closely related article, "An Efficient Workflow for Geological Characterization in Unconventional Reservoirs from a New Through-the-Bit Logging Electrical Micro-Imaging Tool", Search and Discovery article #42334.
 DOI:10.1306/42335Yang2018

[1]Schlumberger, Clamart, Ile-de-France, France (syang4@slb.com)
[2]PetroChina Qinghai Branch, China

Abstract

Accurate structural delineation is very difficult in complex compressional tectonic regimes because of the challenge of seismic processing with large-scale thrust faults. The high-resolution borehole image is commonly the first choice for structural framework construction in such environments. Although we can reconstruct the structural model from borehole image dips, only one fault can be handled in one structural zone in previous traditional methods. Moreover, it is very common that there are multiple faults developed in a vertical or horizontal well, and we cannot build a smooth structural model including multiple faults in one structural zone. In this article, we propose a novel approach to build a two-dimensional structural model with multiple faults from borehole image dips in a challenging compressional stress regime.

First, formation boundary dips are picked from high-resolution wireline logging or logging-while-drilling (LWD) borehole images manually or automatically, in vertical or deviated wells. True-dip based dip picking is applied in horizontal or vertical wells for bull's eye or parallel bedding features. Second, the structural zonation is automatically computed from the formation boundary dip distribution; and the drilling polarity is computed based on the well trajectory and formation dips. Third, the fault truncation relationship is analyzed from the true stratigraphy thickness index, and the potential fault throw is calculated. Last, a novel multiple-fault modeling is applied for one or more structural zones in different structural types, and a structural model is reconstructed by honoring the geological structure and the faults.

Two case studies were used to demonstrate this innovative approach. The first is from a vertical well in a compressional stress regime basin of western China with wireline logging including a high-resolution borehole image. The second is from a horizontal well in a coal bed methane reservoir of Australia with the through-the-bit logging electrical images.

Advanced Dip-Picking Methods from Borehole Image for High Apparent Dips

In a compressional stress regime environment, the apparent dip is very high in most cases. Although this may not pose a problem for determining the dip uncertainty in a vertical well, it does present a significant issue in horizontal wells. More than 10° difference of true dip azimuth could be caused by only 3° difference of apparent dip azimuth.

An improved automatic dip-picking method was newly developed to pick sinusoid dips from borehole images including high apparent dip in both vertical and horizontal wells. More than 300 dips can be picked in 5 minutes, in contrast to hours needed for manual picking (Figure 1).

However, the bed boundaries in highly deviated wells are commonly not normal sinusoids; the traditional dip-picking method cannot be used to pick dips in horizontal wells. A special true-dip-based method was developed to pick features, such as bull's eyes, reverse bull's eyes, and parallel train tracks. The user first picks three points on the borehole image, each point being translated into spatial coordinates (in true dip space), and the triplet defines a spatial plane crossing the borehole to define a dip. The procedure is illustrated in Figure 2. In our example, symmetrical images with certain azimuth range, defined with a dashed cyan line in Figure 2 were used to compute a symmetrical axis. Additional points can be picked along the well by following the image features, and the potential trend is displayed as reference. Then the continuous dip boundaries are picked to match the borehole image features (Figure 2). The color of the symmetrical axis indicates how consistent the current symmetrical axis is compared with the closed interval and helps the user to find the balance between the dip consistency and image feature fitting. The faults are identified manually in both dip-picking methods.

True Stratigraphic Thickness (TST) Computation and Fault Analysis

When the image tool passes through formation layer, the formation boundary can be seen as different features in the image. As shown in Figure 3a, the image shows a bull's eye feature when drilling through a small anticline, which indicates drilling down and drilling up, which is labeled as drilling polarity. The drilling polarity can be computed based on the angle between the well trajectory and the pole of the formation dip as shown in Figure 3b. Drilling down is indicated when this angle is more than 90°, otherwise drilling up is indicated. When the true stratigraphy polarity is normal, the arched pattern ("sad face") represent drilling down, and the upward curve ("smile face") indicates drilling up (Figure 3c). Then, the true stratigraphic thickness is computed from the apparent formation dip and drilling polarity accordingly (Yang et al., 2018).

After the TST computation, the gamma ray (GR) or other log can be displayed with a TST reference. We assume the thickness of formation does not change dramatically in the local area. Correlation is achieved by matching the TST logs across the fault; then, the fault throw can be estimated from the change in TST, and the fault type is classified in sequence (Figure 4).

For the normal fault identification as shown in Figure 4, the TST at the top of formation B is assigned as 0. After TST computation and corrected correlation analysis, the TST is decreasing after crossing the fault boundary along the drilling direction. By considering the dip trend of fault plane, the hanging side of the fault is relatively deeper than down side; thus, the normal fault criteria are matched.

For the thrust fault, the TST at the top of formation A is assigned as 0. The TST is decreasing after crossing the fault plane along the drilling direction but the fault hanging side is relatively shallower than the down side when considering the fault plane, which matches thrust fault criteria.

Structural Modeling with Multiple Faults

In previous popular fault modeling, only one fault could be handled in one structural interval. Having multiple structural zones to handle several faults causes no significant issues in vertical wells because the formation layering is vertically distributed, and we can use the same cross section to reconstruct a smooth structural model. However, it is not possible to have several structural zones in a horizontal well with multiple faults, otherwise the formation layer could not be smoothly maintained and propagated in different structural zones, and the formation layering shows considerable difference in different fault blocks. In most cases, the structural model can only be reconstructed without faults in horizontal wells (Yamada et al., 2016).

To have better cross sections with continuous formation layering in different fault blocks, a novel solution is applied with the following steps (Figure 5). The dips are picked automatically from images in a vertical well (Kherroubi and Maeso, 2016; Ye, 2015; Antoine and Delhomme, 1993) or in a horizontal well with the true dip picking method described above. We can still benefit from the automatic structure zonation and structural axis computation based on great-circle-fitting criteria as in the past. The true stratigraphic polarity is also calculated based on the dip trend in the stereonet.

The fault throw is estimated based on correlation analysis of TST, and the fault type can be identified by combining information from layer tops with the fault dip picked from the image, as explained in the previous section. If the intersection order is not clear when based only on borehole data, the fault ordering is classified by default based on the estimated fault vertical throw; one of the major faults is selected as the main projection plane. All the dips are projected along the major fault plane vertically following similar or parallel fold principles (Etchecopar and Dubas, 1992; Yamada et al., 2016); then, the projected dips are displayed on the plane perpendicular to the structural axis or user-defined cross section plane. If the well trajectory is intersected in the top view and the projected dips can be overlain on the plane perpendicular to the structural axis, then a dip filtering is applied to the projected dips along with the well trajectory. If the cross section is not perpendicular to the structural axis, the projected dips are projected again onto the cross section along with the structural axis.

The fault intersection is built based on fault planes and fault throws, and the formation layers are truncated by the extended fault planes with estimated fault throws. For each truncated area, a B-spline method is applied to make sure the smoothness of each layer.

A Case Study with a Wireline Borehole Image in Vertical Well

In this compressional stress regime, the thrust faults are developed at different scales. One major thrust fault was identified from the regional geology setting, but the fault depth is uncertain based on drilling data. The detailed borehole image features are analyzed to identify the fault depths by integrating bed boundary dip pattern and correlation analysis (Figure 6d). The fault throws are also estimated based on correlation analysis. This is first time to compute fault throw in the same well based on computed TST in this reservoir.

We found that the correlation based on TST index is very useful in this region. As shown in Figure 7, there is no major azimuth change for the fault at depth X154 m (blue circle in Figure 6c), although dip angle is slightly changed around this depth (Figure 6a), and there is no clear fault feature on the borehole resistivity image (Figure 6b). However, we can clearly see the formation duplication on the correlation analysis in Figure 6d, and fault throw is estimated more than 30 m (last row at Table 1).

The seismic data are influenced by this large scale thrust fault order as shown in Table 1, and the interpreted internal structure from seismic does not match the drilling and borehole image data (Figure 8b). With the previous method, six structural zones are classified and reconstructed for the structural model, as shown in Figure 8a. Only one fault or no faults can be modeled in each zone, and the reconstructed model does not represent the real structure. With the new innovative approach, the structural model is rebuilt based on dips picked from the high-resolution resistivity borehole image, which matches the drilling data and offset well information better (Figure 8c). The internal structure is much more complex than the interpretation results from seismic and the fault depths are more confident than in the seismic or conventional log (GR, resistivity, etc.) interpretation. This new near-well structural model provides valuable information for the advanced seismic processing and continuous infill well design.

Second Case Study with the Through-the-Bit Logging Electrical Borehole Image (TBEI) in a Horizontal Well

In a shallow coal bed methane reservoir, the incipient breakouts were identified from a TBEI borehole image. The incipient breakouts are all developed at the top and bottom of hole position with borehole deviation around 90°. This feature indicates that the vertical stress is the minimum stress (Figure 7) and we think that the stress regime in this region is compressional, not extensional.

The bedding boundaries are picked with above methods including sinusoid or non-sinusoid features, as shown in Figure 2. The faults are identified from image features and dip patterns. The TST is computed based on picked bedding boundaries. From the GR pattern displayed in the TST reference, we see that the well trajectory is well placed in the low-GR formation in most intervals bounded by two high-GR formations at top and bottom.

The fault throws are estimated from correlation analysis (Table 2). The fault type is automatically identified based on TST change at fault plane. From Table 2, we find that there are 10 reverse faults developed in this well, and this is a different from the original normal fault prediction, but consistent with the result from compressional stress regime analysis.

The accurate two-dimensional structural model was constructed with multiple reverse faults. After reconstructing the structural framework, the GR log was used for layer filling. As show in Figure 10, the formation layering in cross section matches with the correlation analysis.

To better understand the relationship between the coal cleats and the geological structure, the areal fracture intensity was computed from the borehole image, as shown in Figure 9. We see that fractures are more developed in the low-GR intervals (coal formation), and areal fracture intensity is almost similar in the low-GR formation along the well trajectory. The facture development is not clearly influenced by reverse faults and local structural curvature.

Conclusions

The advanced dip-picking method provides accurate dips with improved efficiency. The TST-based correlation analysis gives the capability of fault type identification and fault throw estimation in a single well. The reconstructed structure from the proposed approach provides more detailed internal information, especially in a compressional stress regime. The results from this innovative method are demonstrated with two wells in different areas with compressional stress regimes. The reconstructed structural model in horizontal wells provides fundamental information for completion design in unconventional reservoirs.

Acknowledgments

The authors thank PetroChina and Schlumberger for allowing us to release the image data and publish this article.

References Cited

Antoine, J.N., and J.P., Delhomme, 1993, Method to Derive Dips from Bedding Boundaries in Borehole Images: SPE Formation Evaluation, SPE-20540-PA.

Etchecopar, A., and M.O. Dubas, 1992, Methods for Geological Interpretation of Dips: SPWLA 33rd Annual Logging Symposium.

Ma, L., Y. Li, G. Wei, S. Yang, T. Yamada, A. He, I. Le Nir, and F. Wu, 2018, A Novel Approach for Structural Delineation with Multiple Faults from High Resolution Borehole Image Dips: Presented at Gastech 2018 Conference & Exhibition, Barcelona, Spain, November 17-20.

Kherroubi, J., and C. Maeso, 2016, Lamination Analysis from Electrical Borehole Images: A Quantitative Workflow: Presented at SPWLA 57th Annual Logging Symposium.

Yamada, T., I. Le Nir, E. Moscardi, and A. Etchecopar, 2016, A New Parallel Fold Construction Method from Borehole Dip for Structural Delineation: Presented at the AAPG Annual Conference & Exhibition, Calgary, Alberta, Canada, June 19-22, 2016, AAPG Search and Discovery Article #90259 (2016). Website accessed December 19, 2018.

Ye, S.J., 2015, A Robust Automatic Dip Picking Technique to Improve Geological Interpretation and Post- Drill Formation Evaluation of Azimuthal Wellbore Image Logs: Presented at the SPE Annual Technical Conference and Exhibition, SPE-175026-MS.

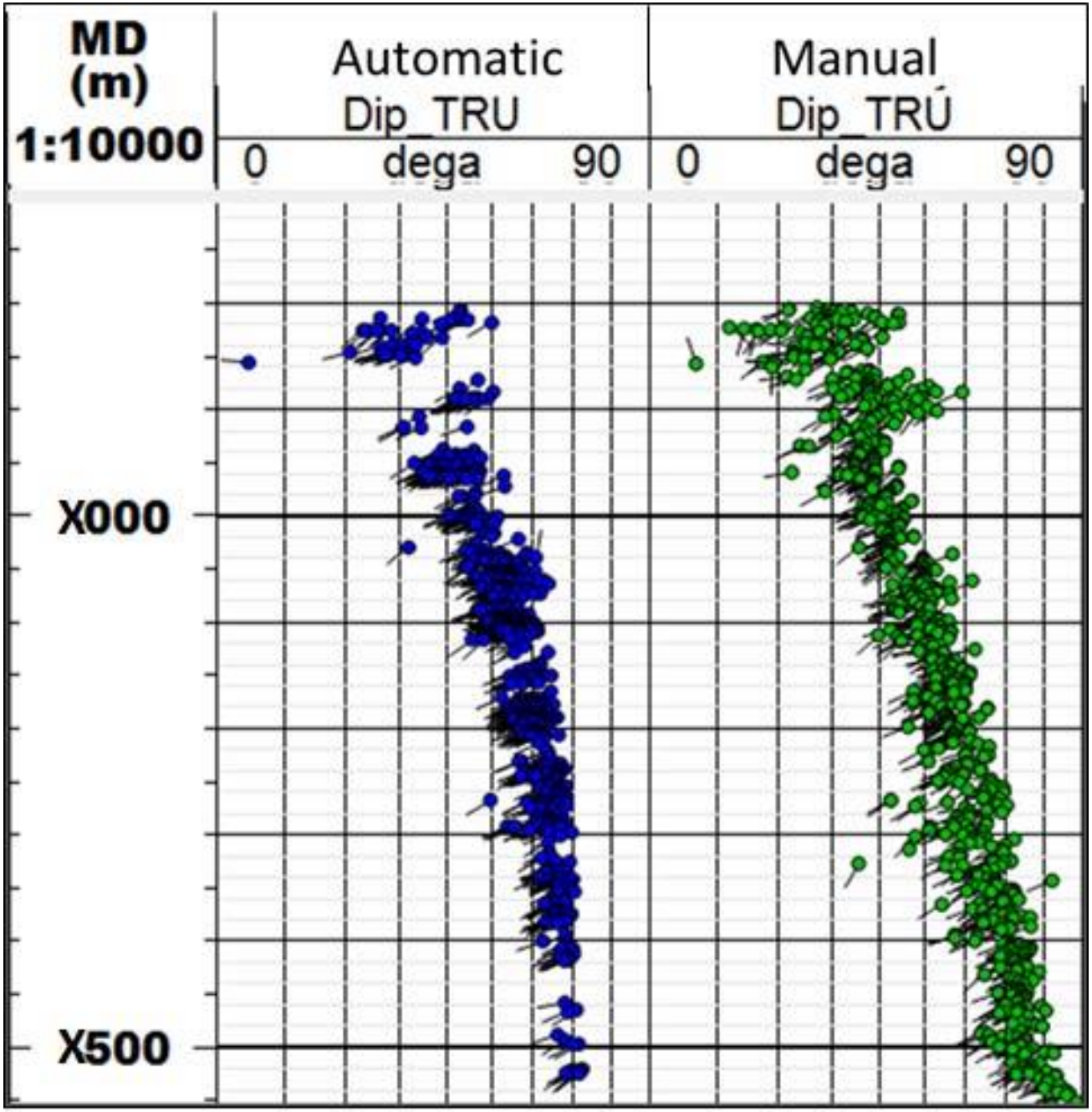

Figure 1. Automatic dip picking from borehole image in vertical well.

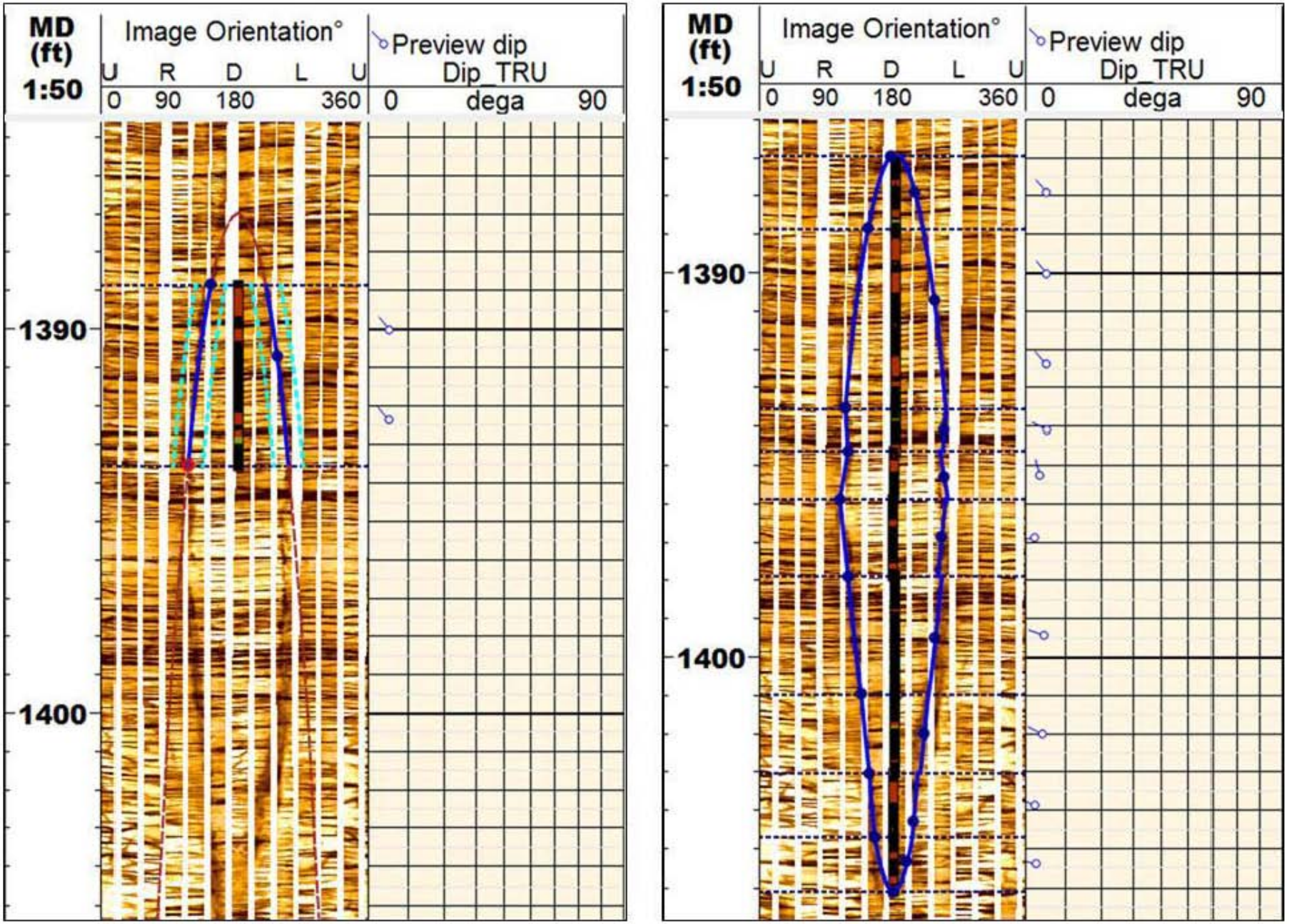

Figure 2. True-dip-based dip-picking in a horizontal well. (a) Define a true dip plane with the first three points. (b) Continue to pick dips by following the true dip plane.

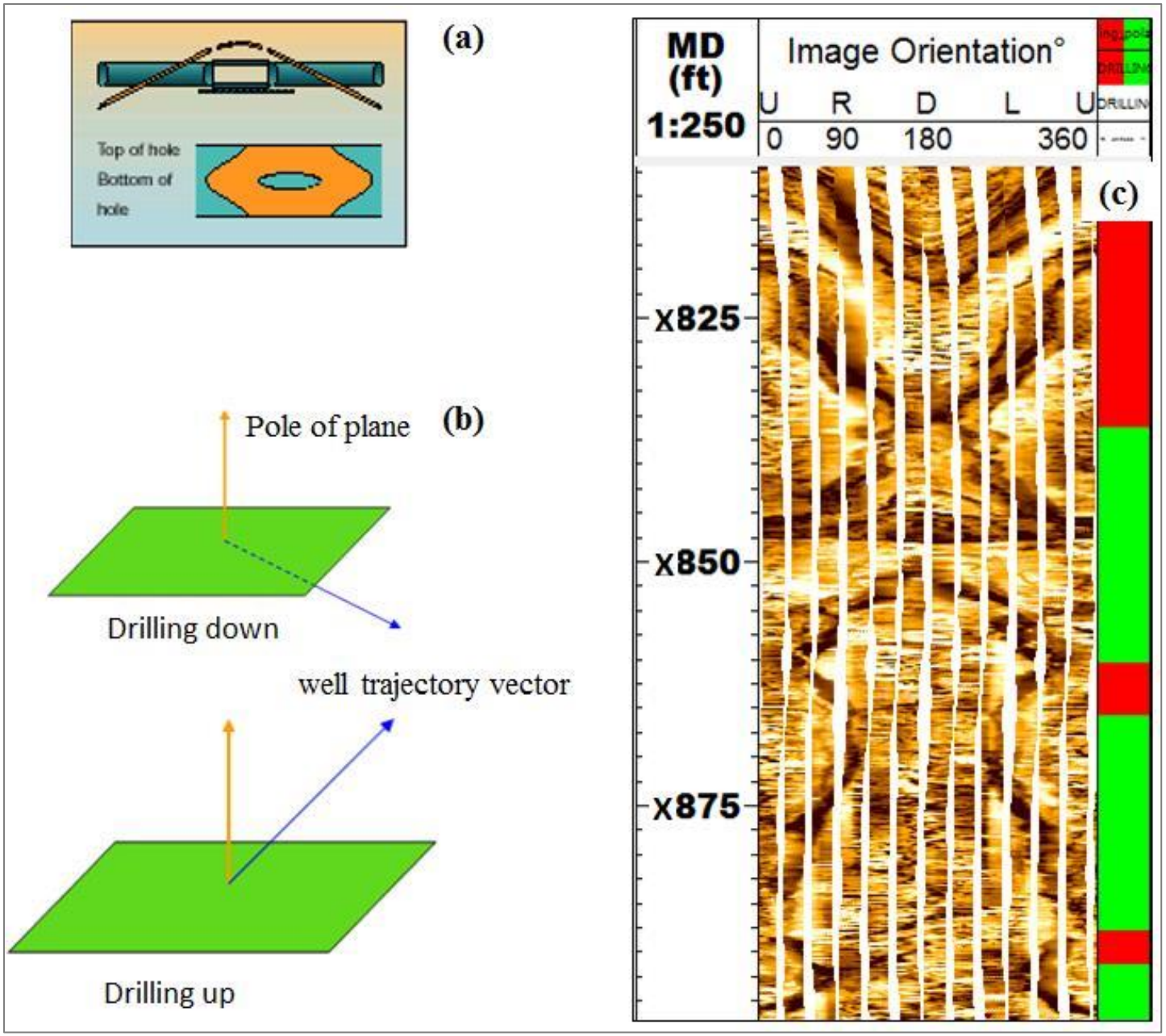

Figure 3. Drilling polarity identification and computation. (a) Sketch map of drilling polarity. (b) Drilling polarity computation from well trajectory and apparent dips. (c) Drilling polarity computation displayed with image features.

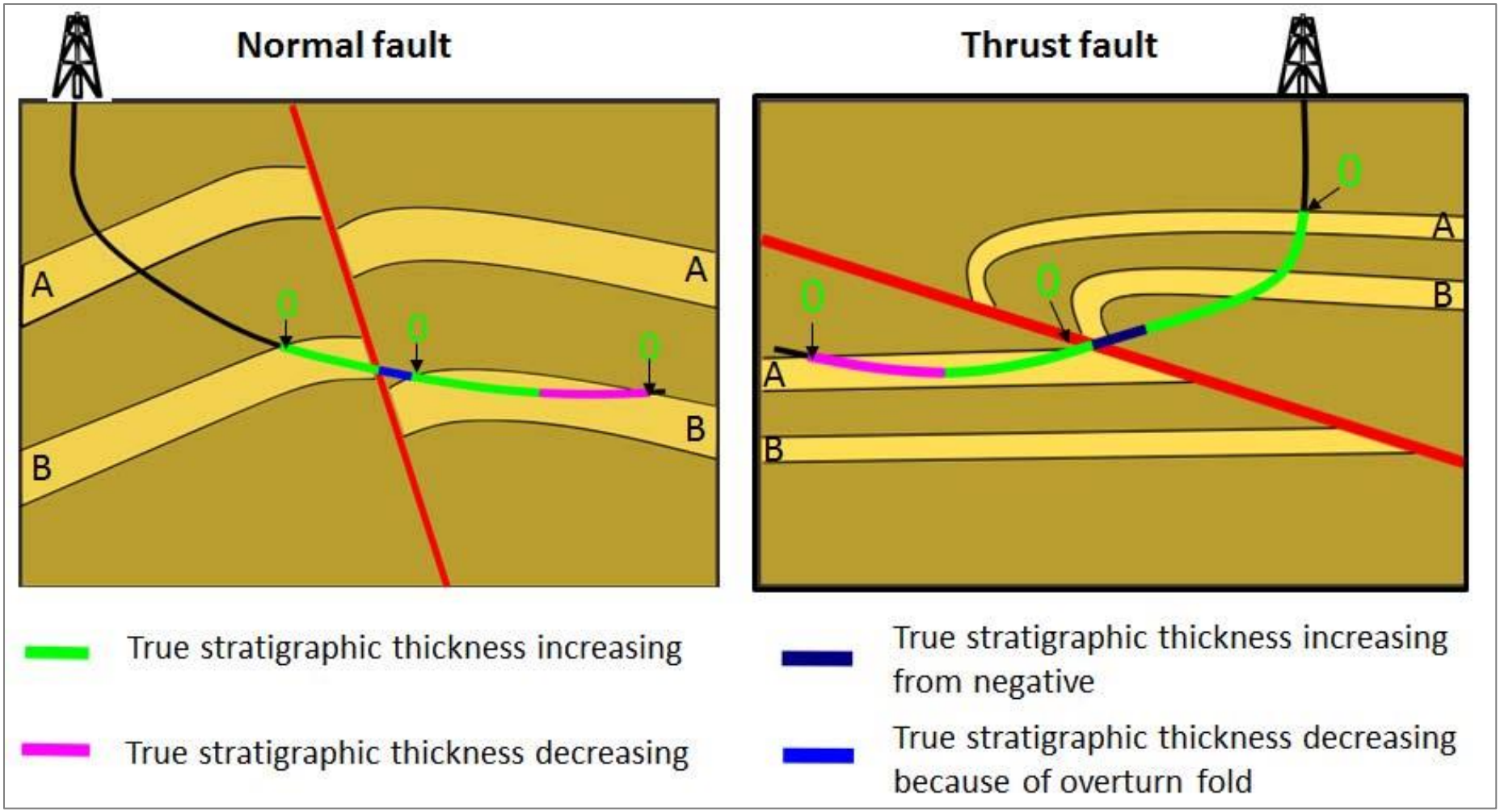

Figure 4. Fault type identification based on TST computation (modified from Ma et al., 2018). (left) Normal fault identification with decreased TST on the upside. (right) Thrust fault with increased TST on the upside. In both cases, the top of the formation marker is assigned to 0 for TST computation.

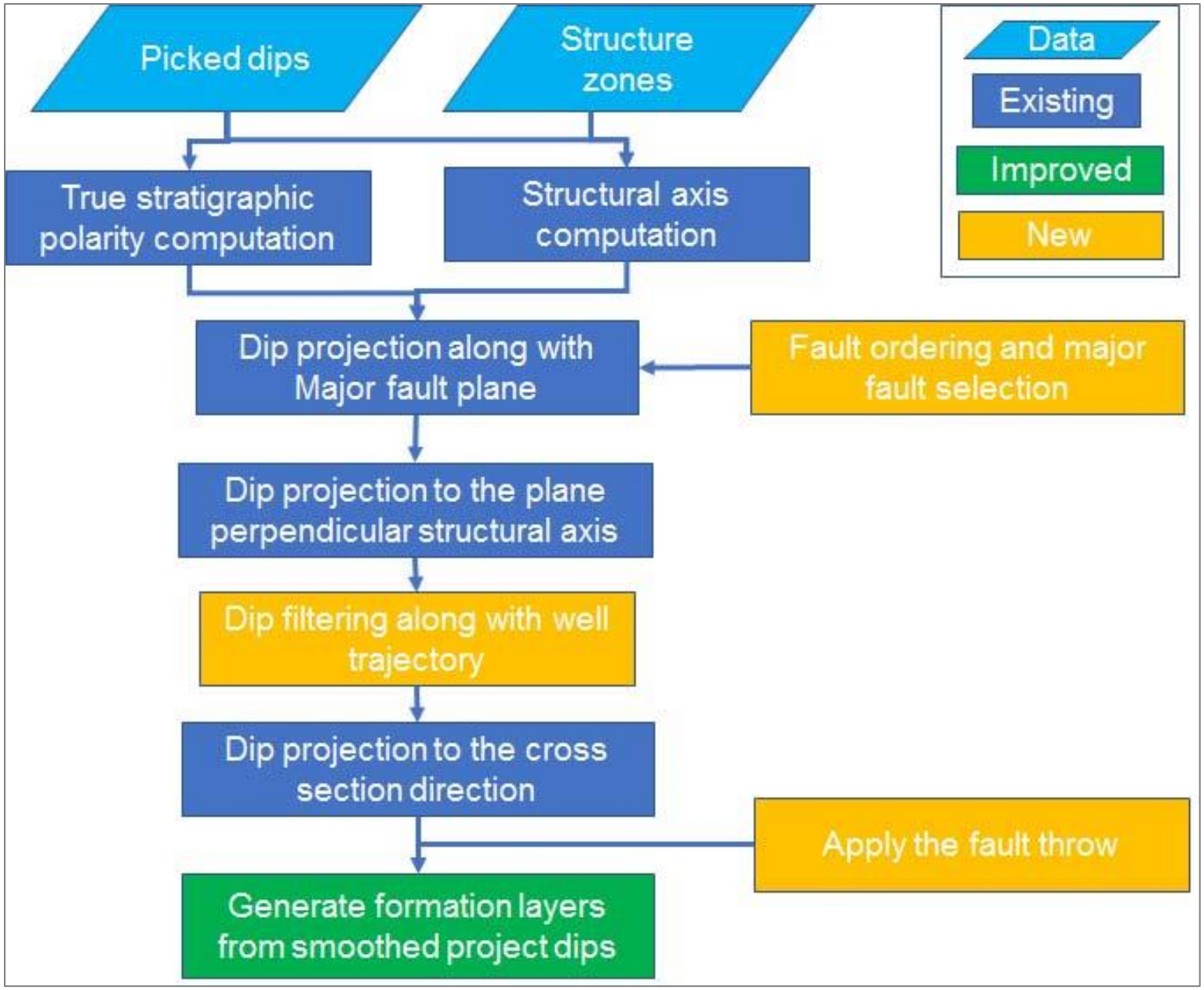

Figure 5. An innovative structural modeling workflow, including multiple-faults modeling (modified from Ma et al., 2018)

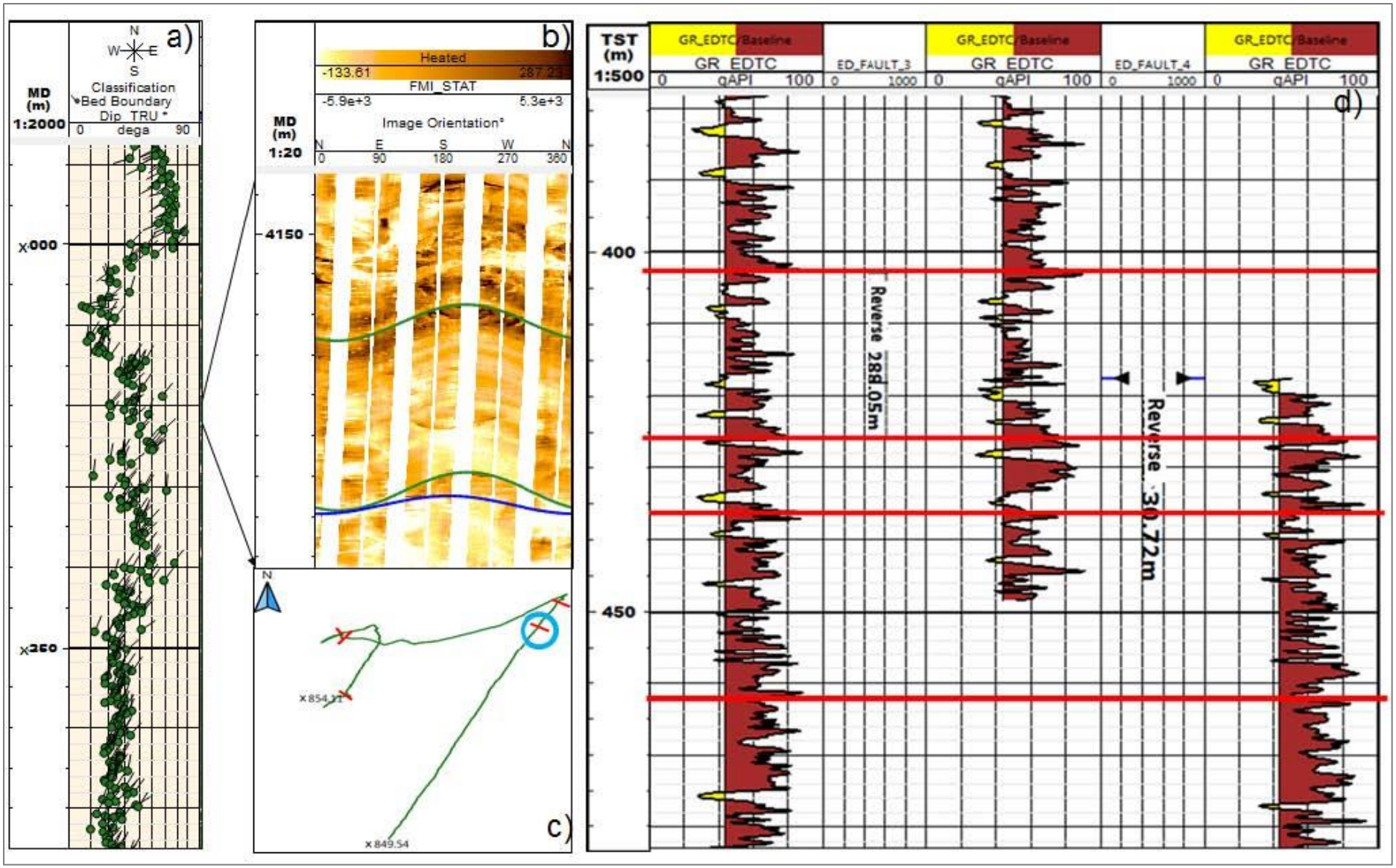

Figure 6. Correlation analysis and fault throw estimation from GR displayed in TST reference. (a) Bedding boundaries. (b) An unclear fault image feature. (c) Fault positions in dip vector plot. (d) A new fault identification in GR display in TST.

MD (ft)	Dip Azimuth	Dip Angle	Fault vertical Throw	Fault Type	Order
X899.076	272.5988	49.5642	45.67	Reverse	4
X154.199	212.2182	56.7007	47.56	Reverse	3
X320.694	222.3678	42.3554	102.34	Reverse	2
X036.291	17.51263	16.3942	286.8	Reverse	1
X151.7	305	24	30.7	Reverse	5

Table 1. Fault throw estimation from correlation analysis.

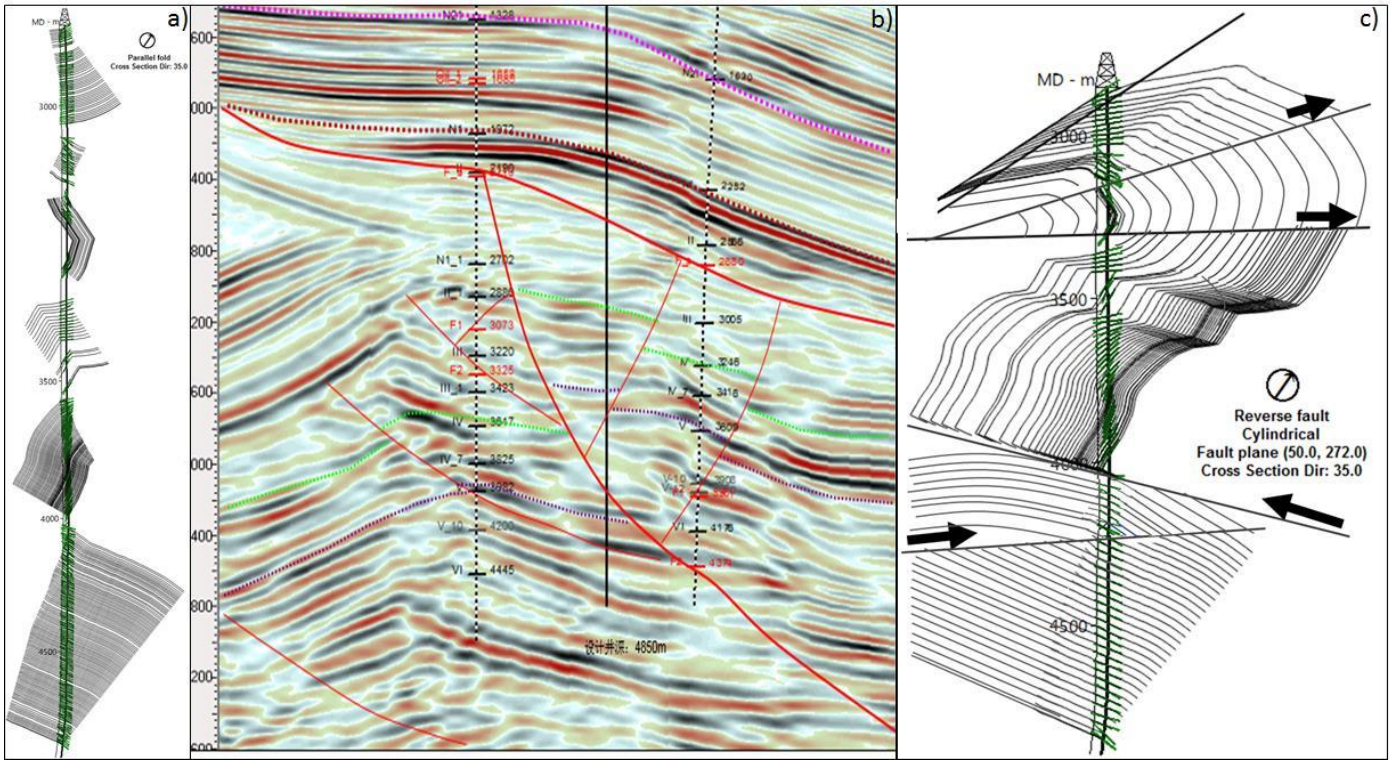

Figure 7. Structural cross section in a vertical well with multiple thrust faults. (a) The previous structural model with six zones. (b) Seismic data and study well trajectory with solid black line. (c) Fault throw estimation from correlation analysis. (d) The new structural analysis result with multiple thrust faults.

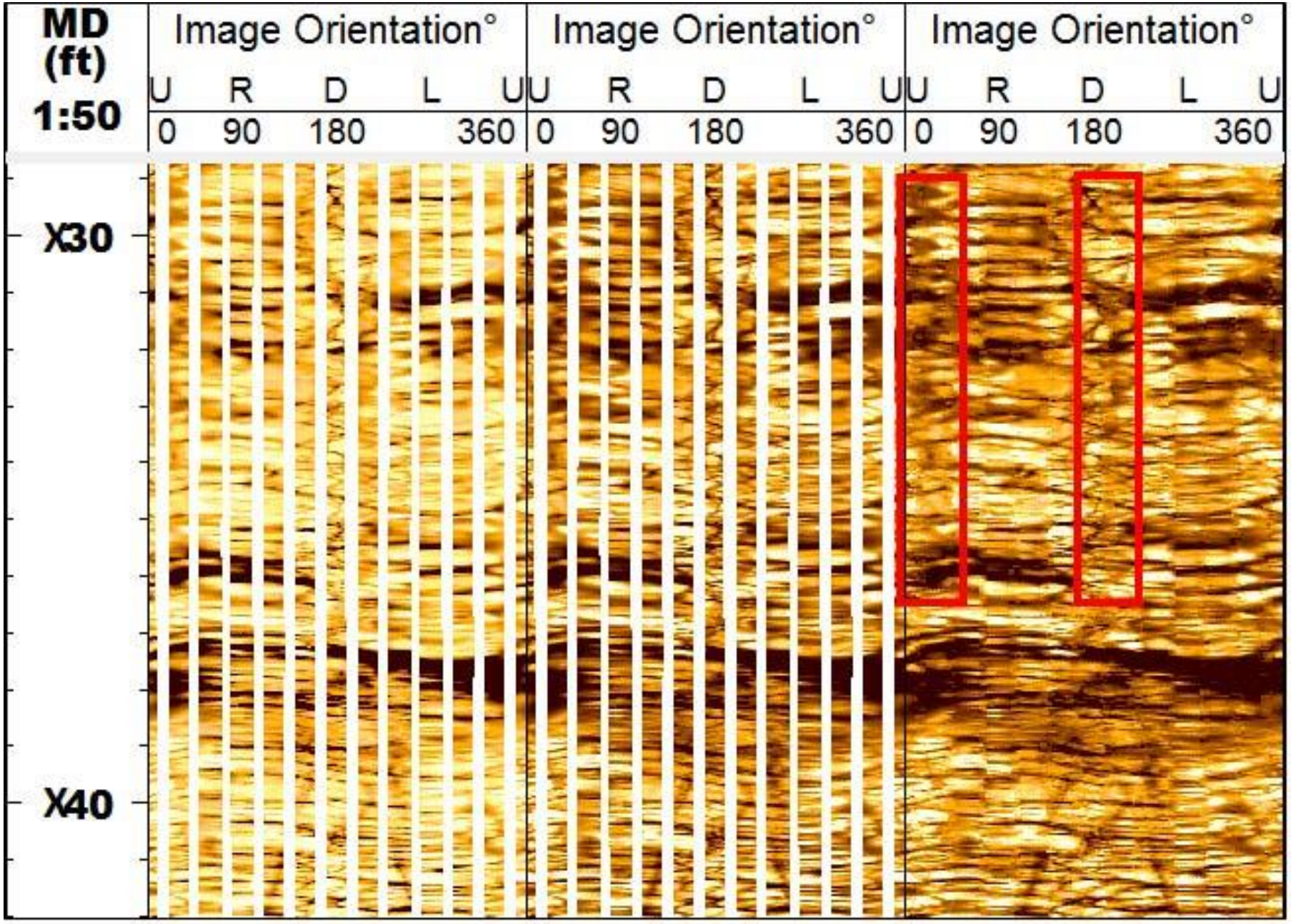

Figure 8. Incipient breakout in different normalized borehole image feature. Track 1, depth track; Track 2, static image; Track 3, dynamic image; Track 4, incipient breakout in reconstructed dynamic image with filled gap.

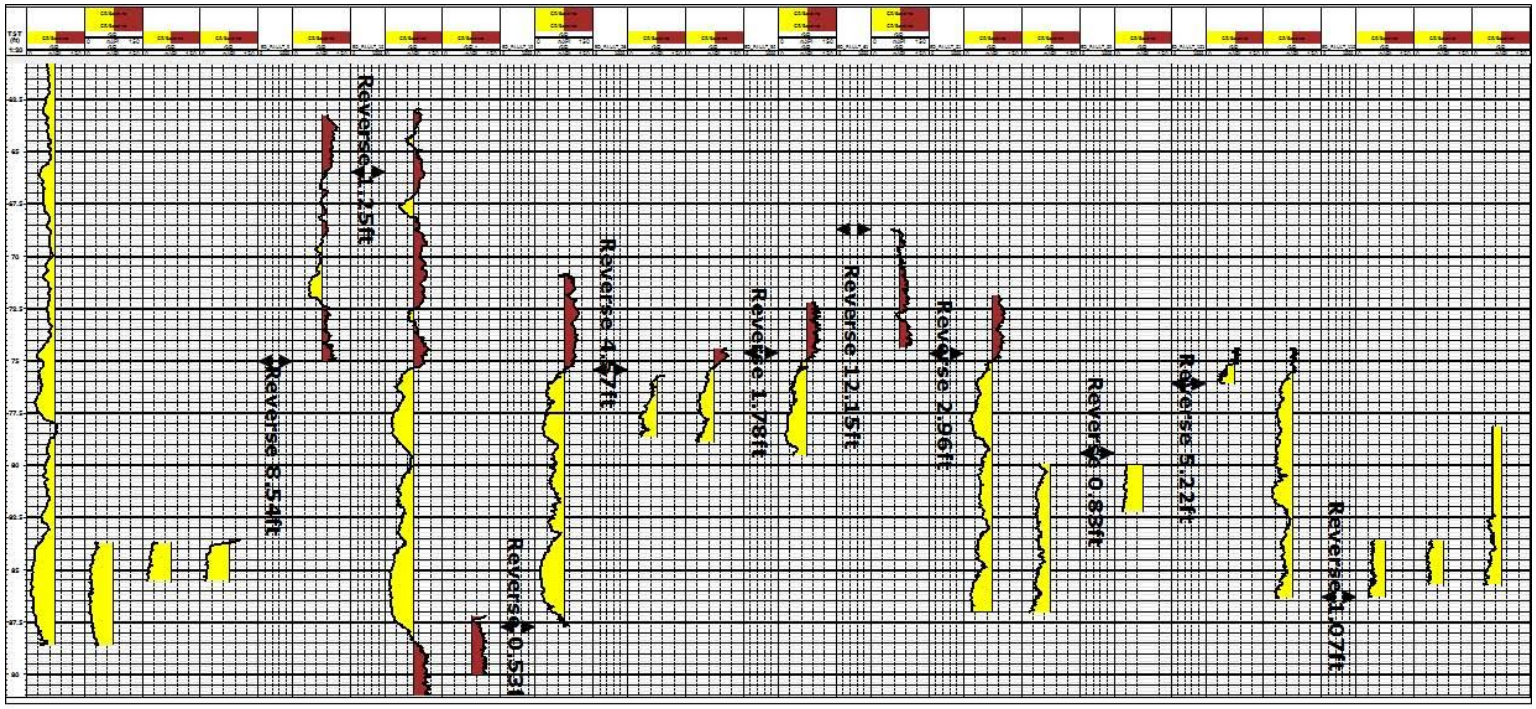

Figure 9. Correlation analysis and fault throw estimation from GR displayed in TST reference.

MD (ft)	Dip Azimuth	Dip Angle	Fault vertical Throw	Fault Type	Order
X429.5	285.47	71.75	8.53765	Reverse	1
X529.184	35.86053	33.69603	1.254266	Reverse	7
X955.378	20.83894	43.80388	0.573603	Reverse	10
X435.49	22.56897	43.7477	4.580654	Reverse	4
X787.883	250.9722	67.56168	1.779876	Reverse	6
X042.257	213.133	62.28463	6.16	Reverse	2
X275.79	65.00551	86.31682	2.988002	Reverse	5
X847.626	235.4185	49.9102	0.830277	Reverse	9
X011.079	235.3968	59.06862	5.271005	Reverse	3
X441.879	328.5278	37.52293	1.076565	Reverse	8

Table 2. Fault throw estimation from correlation analysis.

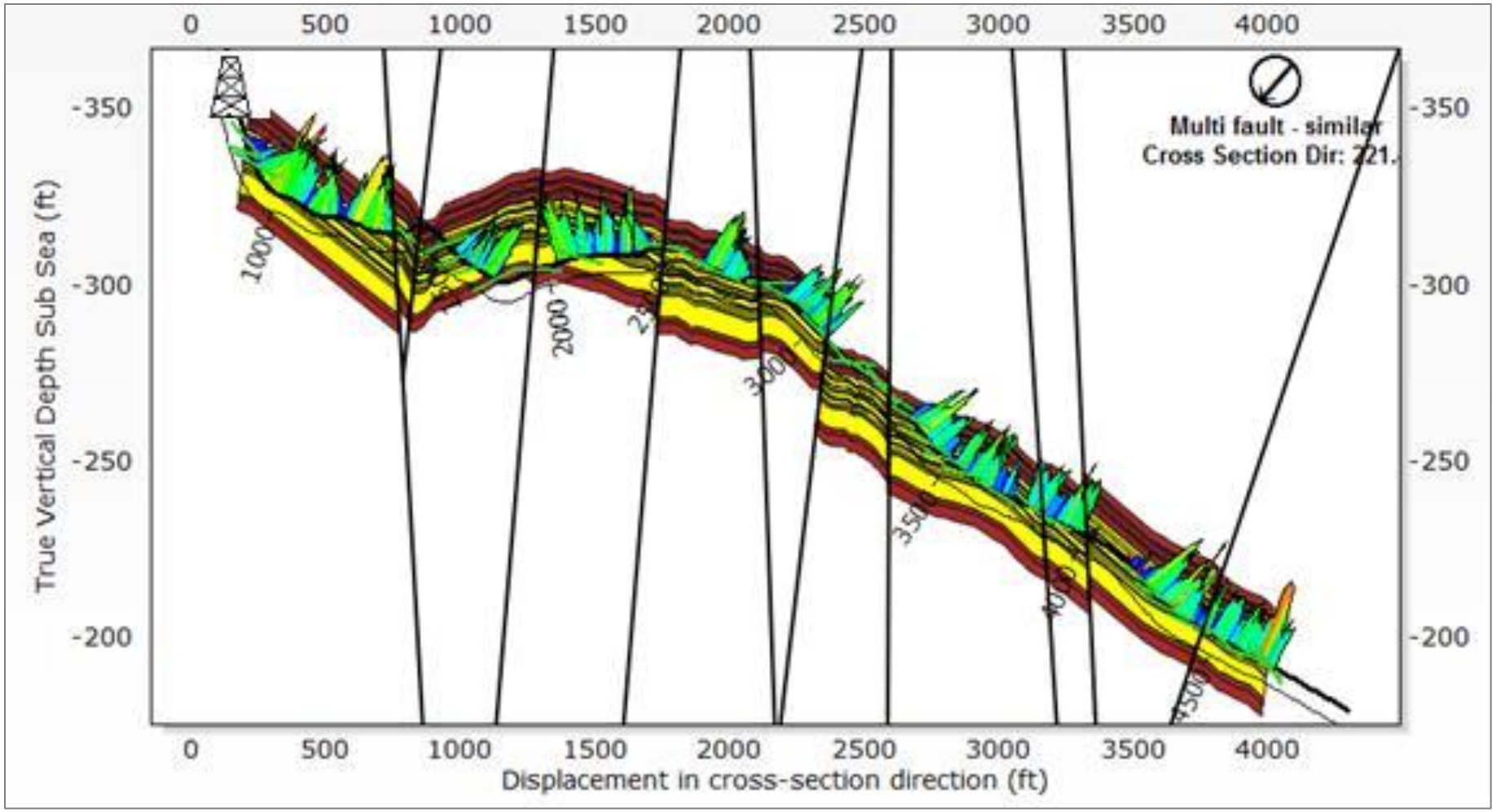

Figure 10. Structural cross section including multiple reverse faults in a horizontal well with areal fracture intensity displayed.